Chemistry–A European Journal
Research Article
doi.org/10.1002/chem.202200129
Chemistry Europe
European Chemical Societies Publishing
www.chemeurj.org

Towards Nitrogen-Rich N-Heteropolycycles: Synthesis of Octaazaperopyrenes (OAPP)

Tobias Wesp,[a] Tim Bruckhoff,[a] Julian Petry,[a] Hubert Wadepohl,[a] and Lutz H. Gade*[a]

Abstract: *Ortho* substituted octaazaperopyrenes (OAPPs) are a new class of functional dyes characterized by their strong electron-accepting behavior. Herein, the synthesis, as well as the electrochemical and photo physical properties of an OAPP dye, is reported. The OAPP target was prepared via selective nucleophilic substitution at the *peri* position of a *bay* chlorinated tetraazaperylene by introduction of four amino-substituents. The resulting tetraminoperylene was reacted with different acyl chlorides and anhydrides to give the twisted *bay* chlorinated OAPP derivatives which were isolated in their reduced dihydro-form. The OAPP target could be obtained via a palladium catalyzed dehalogenation and a subsequent oxidation. The eightfold isosteric [CH→N] replacement within the peropyrene core structure results in a large decrease of the frontier orbital energies, rendering the target compound a potent oxidant while preserving the planarity of the aromatic core. The radical anion was obtained by reduction of the OAPP with KC_8 and characterized by EPR spectroscopy. A general discussion of the number and location of [CH→N] replacements in peropyrene structures and their frontier orbital energies is provided.

Introduction

The use of functional dyes as electronic materials has led to a revival of the chemistry of polycyclic aromatic compounds.[1–7] Interesting in their own right due to fine tunable photophysics and redox properties in solution, their properties as conducting solids has significantly driven this development.[8–9] While there are nowadays many organic *p*-semiconducting materials with high charge carrier mobilities, which can be used for the OFET technology,[10–11] the performance of *n*-semiconducting materials based on molecular compounds with electron acceptor properties remains to be improved.[12–13] One strategy towards new electron acceptors is the isosteric replacement of CH-units by nitrogen atoms within the polycyclic aromatic cores, thus lowering the energies of the frontier orbitals, in particular the LUMOs.[14–16] This approach has been extensively studied in acene chemistry and shown to convert the typical *p*-semiconducting materials into an *n*-semiconducting material.[6,15,17–20]

The synthesis of N-heteroacenes has a long history. In pioneering studies by Hinsberg[21] as well as Hepp and Fisher[22], the first oligoazaacenes were synthesized and characterized. The tetracenes which were obtained in the reduced form (NH-compounds) were easily oxidizable, a step which proved more challenging for condensed aromatics (e.g., dihydronaphthazine).[23–24] The oxidation of larger azaacenes with acidic dichromate generally results in the corresponding quinones[25] which allows the synthesis of alkynylated azaacenes by a nucleophilic reaction with lithium acetylides and a subsequent full aromatization with $SnCl_2$.[19,26–27]

To date, many azapentacenes[28–30] and larger acenes[31–33] have been synthesized which are strong electron acceptors and exhibit *n*-semiconducting behavior.[3–6,14,17–18,34–35] These studies have revealed that the position of the nitrogen atoms in the aromatic core plays an important role in influencing the semiconducting properties, electronic structure and molecular packing.[17–18,36] Additionally, computational studies have been carried out to model the materials properties and to analyze the influence of the isosteric [CH→N] replacement.[15–16,20, 37]

We systematically investigated the chemistry and properties of tetraazaperopyrenes (TAPP) as electron accepting functional dyes which were found to possess similar electrochemical and photo physical properties but distinctly different reactivity compared to the extensively studied perylenediimides (PDIs).[38–51] In contrast to the PDIs, the electron accepting character of the TAPP derivatives arises from the fourfold isosteric replacement [CH→N] and not the addition of strong electron withdrawing groups like the carboximide substituents.[48] In this way, the strong electron accepting behavior and the resulting electronic materials properties are introduced into the aromatic core without changing the molecular shape.[38]

In TAPP molecules, the electrophilic substitution of the parent compound (e.g., bromination) occurs solely in the *ortho*-position[43,45] whereas the PDIs react in the *bay*-position[2,52–55]. Numerous derivatives of the TAPP substituted in the "axial" 2, 9-positions[38,42] and in the *ortho* positions[43–44,56–57] have been

[a] *T. Wesp, T. Bruckhoff, J. Petry, Prof. H. Wadepohl, Prof. L. H. Gade*
Anorganisch-Chemisches-Institut
Universität Heidelberg
Im Neuenheimer Feld 270, 69120 Heidelberg (Germany)
E-mail: lutz.gade@uni-heidelberg.de

Supporting information for this article is available on the WWW under https://doi.org/10.1002/chem.202200129

studied for more than a decade which has provided detailed insight with regard to their electronic and photophysical properties and allows reliable predictions of their behavior.

Additionally, we recently developed a synthetic approach to functionalize the *bay*-position which made the *bay* chlorinated and perhalogenated TAPPs accessible,[48–50] while the planarity of the aromatic core is lost due to the steric pressure. Finally, perhalogenation of the TAPP core (Scheme 1) leads to further reduction of the LUMO energy and improved electron acceptor properties, rendering radical anions and dianionic species isolable.[50]

In this work, we expand the concept of the isosteric [CH→N] replacement to further reduce the HOMO and LUMO energies of a polycyclic aromatic system[58] without addition of acceptor substituents.[59] The aim is an access to a powerful electron acceptor, without significant changes in the molecular shape of the molecules, in particular, loss of the planarity of the aromatic core.[17,59] Based on the peropyrene scaffold as point of reference, we developed the synthesis of a novel N-atom rich octaazaperopyrene, thus containing four additional nitrogen atoms compared to the TAPP system. We also focused on the characterization of the corresponding reduced compounds, including the isolation of the radical anion, to gain further insights into its electronic behavior and stability of this new class of organic functional dyes.

Results and Discussion

At the beginning of this study we performed a computational screening of a range of different azaperopyrenes derived from the TAPP reference system[38] by successive [CH→N] replacement. This was meant to assess the effect of such modifications within the "structural space" of the peropyrene core and to assess potential synthetic N-atom rich target compounds gauged on the basis of their potential properties and stability.

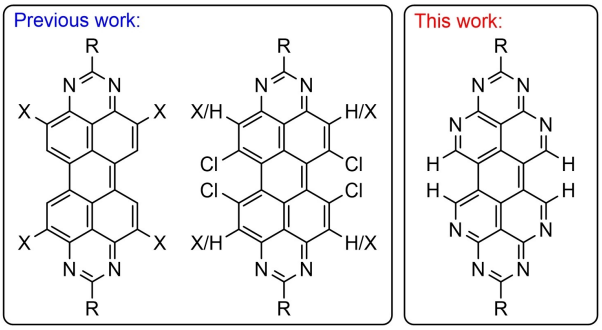

Scheme 1. Previously synthesized *ortho* and *bay* substituted TAPPs (left) and the approach to synthesize an OAPP (right).

Computational modeling of the frontier orbital energies of n–azaperopyrenes (n = 4–8)

A useful approach for a computational screening of the electron acceptor properties of polycyclic aromatic compounds is based on readily calculated LUMO energies. For the non-substituted tetraazaperopyrene TAPP the LUMO energy was previously determined to be significantly higher than the work function of gold,[38,42–43] which is widely used as the standard testing electrode for organic transistors.[10] Further decrease of the LUMO energy of TAPP was based on isosteric replacement of CH-units with nitrogen atoms in the peropyrene core, and to this end we modeled the frontier orbital energies screening a set of polyazaperopyrenes by means of DFT at the B3LYP/Def2-TZVPP-GD3(BJ)[60–66] level of theory (see Supporting Information for details). As validated in previous studies on tetraazaperopyrenes,[38,43–45] the chosen functional/basis set combination is suitable for a direct comparison of the DFT-LUMO energies with the work function of gold and generally gives rise to a good agreement between calculated and experimentally derived frontier orbital energy dependent properties (see below).

The comparison of the known tetraazaperopyrene derivatives with an electron withdrawing perfluoroalkyl group (CF_3) and an electron donating alkyl group (CH_3) at the 2- and 9-positions revealed a difference of ~0.6 eV of the LUMO energy.[38,43] Since both series of derivatives were assumed to be equally accessible, the energetically more stabilized 2,9-Bis(trifluoromethyl)-1,3,8,10-tetraaza-peropyrene (CF_3-TAPP) was chosen as reference system for a computational screening, with up to four additional nitrogen atoms to be incorporated in the polycyclic aromatic core. Since perylene cores with vicinal nitrogen substitution are known to be challenging to synthesize,[67] only those peropyrenes without vicinal nitrogen atoms were considered (for the full screening, see below and Supporting Information).

Beginning with the known TAPP reference system,[38,43] the expected trend towards lower frontier orbital energies was found upon increasing the number of nitrogen atoms in *ortho* and *bay* position, with the latter having a smaller effect (Figure 1). This can be explained by the larger orbital coefficients of the frontier orbitals in the *ortho* position of the TAPP, as well as slightly higher Mulliken charges at this position (see Supporting Information, Figure S1).[38] Generally, we found a linear correlation between the number of [CH→N] replacements and the frontier orbital energies which were modeled only for the cases of purely *bay* or *ortho* N-substituted derivatives while mixed patterns were not considered at first. This observed linearity is due to the shape of the frontier orbitals being nearly independent of the specific aza substitution and reflected in the different *bay* and *ortho* N-substituted constitutional isomers of hexaazaperopyrene delivering nearly the same frontier orbital energies.

Notably, the HOMO-LUMO gap (ΔSCF) was slightly reduced with increasing nitrogen substitution in the *bay* positions. Therefore, an *ortho* [CH→N] replacement appeared more attractive in an initial synthetic approach as a larger HOMO-

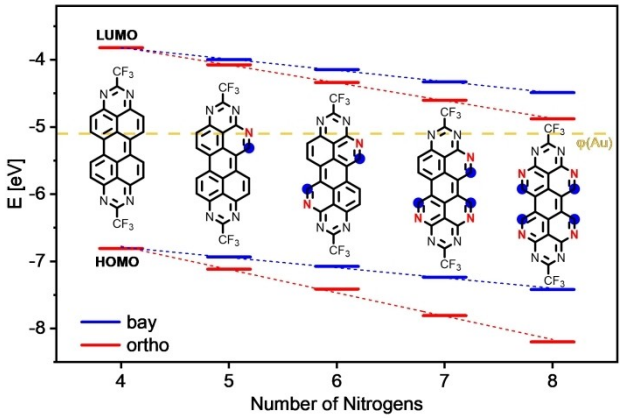

Figure 1. Calculated HOMO and LUMO energies of different *ortho* (N in red) or *bay* (blue circles) substituted peropyrenes derived from TAPP are displayed (B3LYP/Def2-TZVPP-GD3(BJ)). The aza substitution was modeled only for the cases of exclusive *bay* or *ortho* [CH→N] substitutions while mixed patterns were not considered. For the hexaazaperopyrene only one of the three constitutional isomer is displayed all of which were found to possess very similar frontier orbital energies.

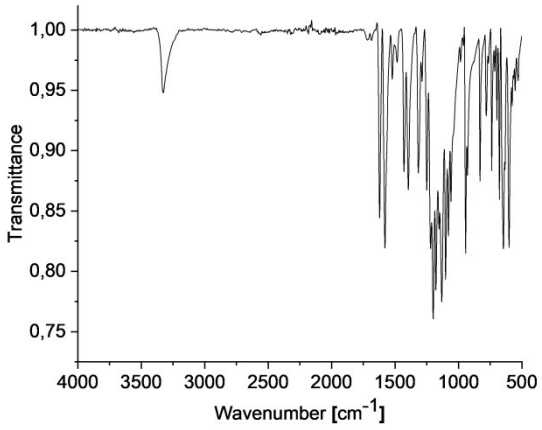

Figure 2. IR spectrum of compound **7 a** with a NH-peak at 3325 cm^{-1}:

LUMO energy gap was thought to lead to more stable electron acceptor materials.[68–70] We therefore chose the planar, *ortho* azasubstituted octaazaperopyrene (OAPP), representing the extreme, as first synthetic target in this context.

Synthesis of octaazaperopyrene

As the starting material for the synthesis of octaazaperopyrenes (**OAPP**) we employed the inexpensive 1,3-acetonedicarboxylic acid diethyl ester. The naphthyridine structure is generated by a Knoevenagel reaction followed by an intramolecular cyclization (Scheme 2).[71] Campbell *et al.* observed that compound **2** dimerized under ambient aerobic conditions and that this reaction could be accelerated by adding H_2O_2 to obtain the perylene structure.[72–73] The almost insoluble blue compound **3** could be activated for further transformation by converting the hydroxy groups to chlorosubstituents, as first described in 1991 by Höchstetter.[74]

The octachloro tetraazaperylene **4** was found to be highly reactive towards nucleophiles, and the nucleophilic attack of primary amines or alcohols to take place in the *peri*-position selectively.[74] 4-Methoxybenzylamine was used to introduce the amino function in the *peri* position giving compound **5**, which was subsequently deprotected by refluxing in TFA according to a similar literature procedure.[75] Finally, the tetraamine **6** reacted with acyl chlorides under the standard reaction conditions[43] previously established for the TAPP synthesis to form the octaazaperopyrene structure in **7 a**–**f**. The ^{1}H NMR and the IR spectra Figure 2) indicated that the resulting compounds were generated in their reduced form with two of the overall eight nitrogen atoms bearing a proton. In the next step, the electron density of the azaperopyrene core was increased by a palladium catalyzed dehalogenation[76] of the *bay* chlorinated

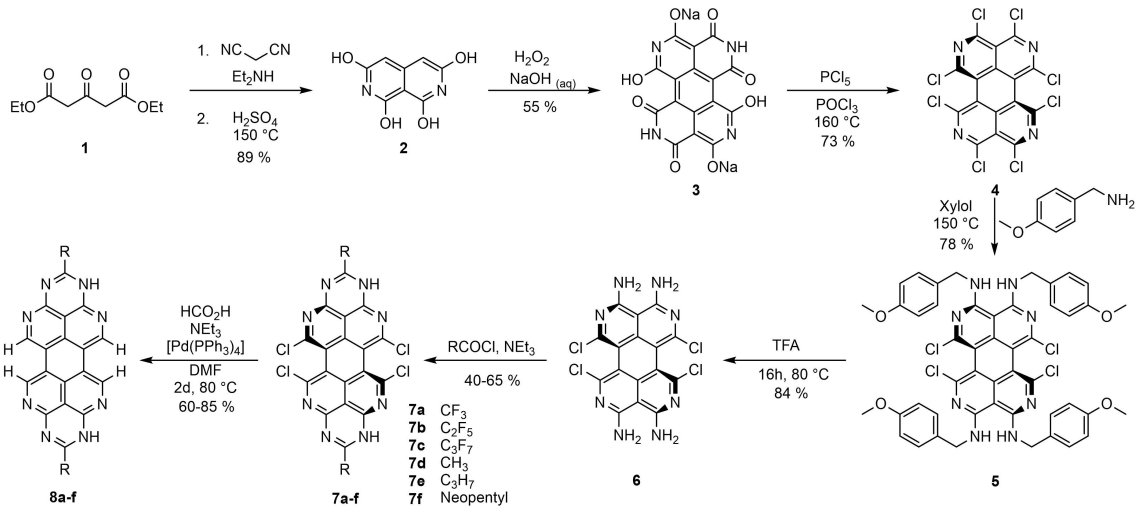

Scheme 2. Synthetic route to the OAPP.

derivatives **7a–f**, which resulted in a planarization of the perylene core. Similar to **7**, compounds **8a–f** were isolated in their reduced (formally hydrogenated) state. All of the compounds **8a–f** were only sparingly soluble in common solvents which is to be viewed as resulting from the planarization of the polycyclic aromatic cores and the capability to form intermolecular H-bonds.

Finally, compound **8c** was oxidized with MnO_2 to give the target OAPP **9c** (Scheme 3). To avoid decomposition, the oxidation was carried out under argon atmosphere. The OAPP is not stable at r.t. and can be handled only for a few minutes under argon atmosphere. Only compound **9c** was isolated as a pure compound due to the thermal instability of the OAPPs in their oxidized form. For all the other derivatives, unspecific decomposition was observed during the oxidation.

Crystal structures

Single crystal X-ray structure analyses of the twisted dihydro-OAPP **7a** and the protonated, unsubstituted dihydro-OAPPs **8a** and **8e** were obtained from hot concentrated solutions in ethanol (**7a**), sulfuric acid (**8a**) and $HCl_{(aq)}$ (**8e**). The structural data of **7a** confirm that the compound is in the reduced state. The NH proton forms a hydrogen bond (1.81 Å) with an ethanol molecule. As a *bay* chlorinated derivative **7a** displays a significant twist of 33.7° (θ) between the tetraazaphenalenyl subunits of the peropyrene core which results from steric pressure of the four chlorine substituents (Figure 3).[48] This observed twist is comparable to that of the *bay* chlorinated TAPP (29.4°–32.4°) as well as structurally similar PDIs.[48,77] The C–C bonds between the two tetraazaphenalenyl units have a length of 1.47 Å which is longer than for the phenalenyl units of the corresponding *bay* chlorinated TAPP (1.42 Å) and longer than typical aromatic C–C-bonds.[48] This suggests incomplete delocalization of the π-electrons over the peropyrene core. The individual tetraazaphenalenyl units are also strained because of the twist, resulting in the increased bond length between C10 and C17 (1.45 Å) compared the other aromatic C–C bonds (1.38–1.40 Å). The packing pattern in the solid state shows an intermolecular π–π-stacking of two adjacent tetraazaphenalenyl units with a plane distance of 3.5 Å, leading to a slipped-stack packing pattern (Figure 3c).

The crystal structure of the dehalogenated, protonated OAPP $[H_2\mathbf{8a}]^{2+}$ was determined and revealed that this compound also was in the reduced dihydro state. The acidic medium (H_2SO_4) was employed for crystal growth because the planarized molecular compound resulting from the hydrodechlorination step proved to be only sparingly soluble in common organic solvents. Consequently, this OAPP derivative **8a** is twice protonated in the isolated hydrogensulfate salt. Analogous to compound **7a**, which was hydrogen bonded to a solvent molecule, the proton of the NH group forms a hydrogen bond with the hydrogensulfate counterion (distance: 2.14 Å). As confirmed in the X-ray diffraction study, the dehalogenation has led to a planarization of the peropyrene core (Figure 4b), which is rendered similar to the unsubstituted TAPP.[38] The

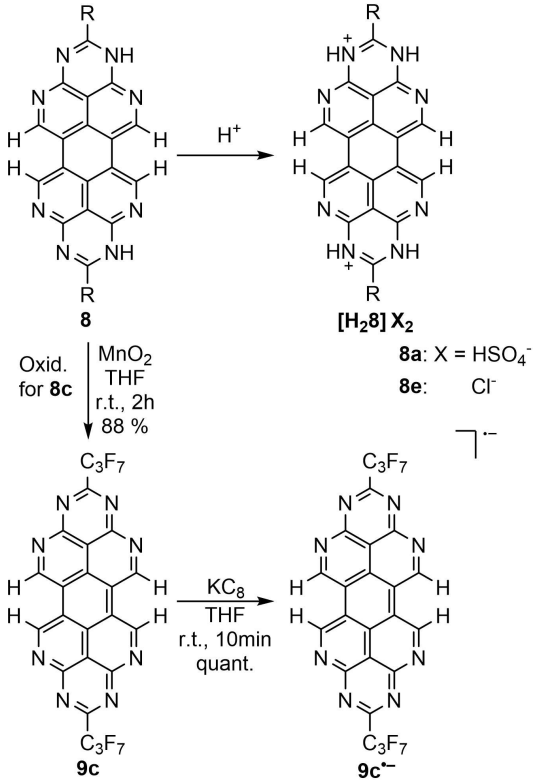

Scheme 3. Synthesis of the OAPP **9c** by the oxidation with MnO_2 (left) and the reduction with KC_8 to the radical anions (bottom); protonation of compounds **8a** and **8e** with $HCl_{(aq)}$ or H_2SO_4.

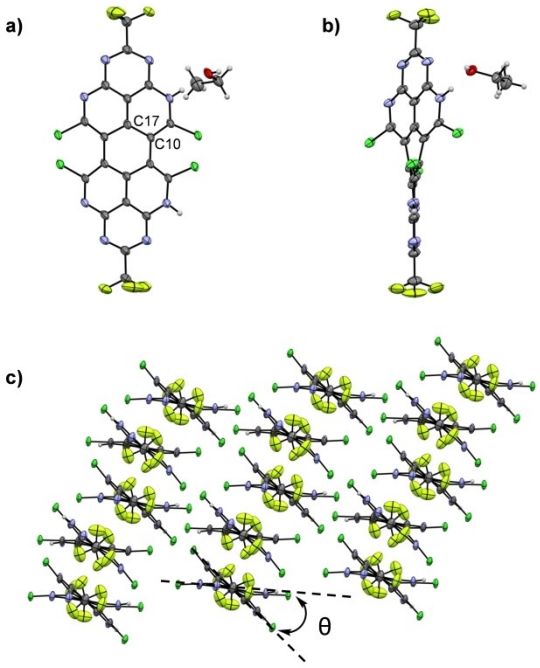

Figure 3. Solid state structure of **7a** co-crystallized with ethanol from top view (a) and side view (b); the slipped-stack packing pattern of **7a** determined by the intermolecular π π stacking of two tetraazaphenalenyl subunits (c) (the solvent molecules are omitted for clarity).

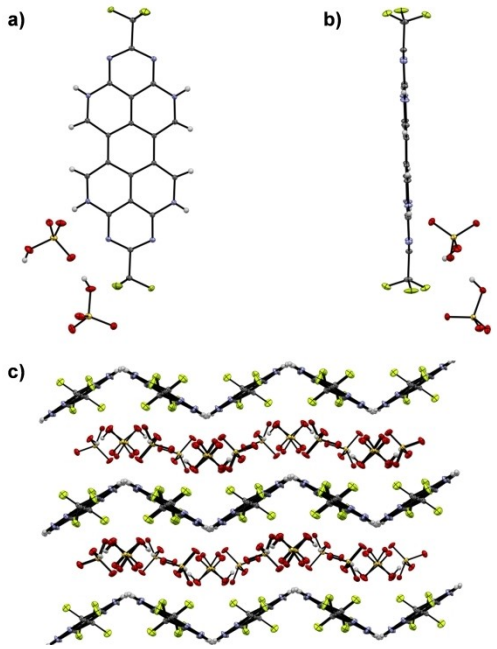

Figure 4. Solid state structure of $[H_2\mathbf{8a}]^{2+}$ crystallized in sulfuric acid from top view (a) and side view (b); the compound exhibits a zigzag packing pattern with alternating layers of $[H_2\mathbf{8a}]^{2+}$ and hydrogen sulfate (c).

planarization results in a reduction of sterical stress in the naphthyridine core and consequently the bond length between C10 and C17 decreases to 1.42 Å. The other bond lengths are nearly identical compared to compound **7a**, for instance, the C–C bond length between the two tetraazaphenalenyl units remains at 1.47 Å. OAPP **8a** packs in a zigzag packing pattern with a π-π distance of 5.96 Å. The large π-π distance results from an alternating sequence of an OAPP layer and a hydrogen sulfate layer in the solid state structure (Figure 4c).

Apart from these two perfluoralkylated derivatives, single crystals were obtained for the protonated 1,9-dipropyl derivative $[H_2\mathbf{8e}]^{2+}$ (Figure 5a) from an aqueous solution of HCl. Although alkylation increases the electron density compared to the perfluoroalkylated derivatives and would thus destabilize the reduced state, the solid state structure of compound **8e** also confirmed the dihydro form in this case. The C–C bond length for the C10-C17-bond is again 1.47 Å and, as with compound **8a**, a planar peropyrene core was observed. Analogous to compound $[H_2\mathbf{8a}]^{2+}$, discussed above, the dihydro OAPP **8e** is protonated twice. Despite the formal similarity to compound $[H_2\mathbf{8a}]^{2+}$ as an AB_2 salt, a very different crystal structure was found, namely a slipped-stack packing pattern for OAPP $[H_2\mathbf{8e}]^{2+}$ (Figure 5c) with a short π-π distance of 3.38 Å due to intermolecular stacking via two tetraazaphenalenyl units. The key data of the solid state structures are summarized in Table 1.

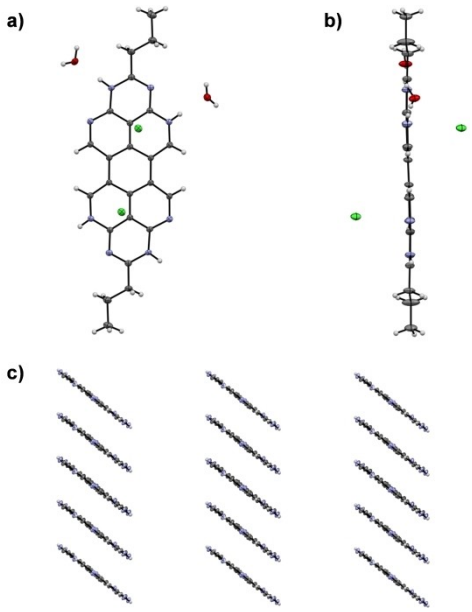

Figure 5. Solid-state structure of $[H_2\mathbf{8e}]^{2+}$ crystallized in hydrochloric acid from top view (a) and side view (b); the packing pattern delivered a slipped-stack packing pattern (c) (the solvent molecules are omitted for clarity).

Table 1. Structural parameters of solid-state structures of **7a**, **8a**, and **8e**.

	Crystal system	Space group	π-π Plane distance [Å][a]	Torsion Angle θ [°][b]
7a[c]	triclinic	P-1	3.517	33.7(4)
$[H_2\mathbf{8a}]^{2+}$[d]	monoclinic	$P2_1/c$	5.956	4.22(13)
$[H_2\mathbf{8e}]^{2+}$[e]	triclinic	P-1	3.380	1.4(3)

[a] π-π plane distance was measured between two adjacent tetraazaphenalenyl subunits. [b] Torsion angle was measured between both tetraazaphenalenyl subunits of one molecule. [c] **7a** co-crystallized with ethanol. [d] $[H_2\mathbf{8a}]^{2+}$ crystallized as hydrogen sulfate. [e] $[H_2\mathbf{8e}]^{2+}$ crystallized as chloride.

UV/Vis absorption and emission spectra

The UV/Vis spectra and emission spectra of the R-OAPP-Cl (**7a**–**f** in THF), R-OAPP–H (**8a**–**8f** in TFA) and **9c**, (in THF) are displayed in Figure 6. Similar to the TAPP derivatives, the absorption maxima are nearly constant within the respective series of 1,9-bisperfluoroalkyl or 1,9-dialkyl derivatives.[43,45] Overall, the perfluorination of the alkyl chains results in a shift of the absorption maxima of 35 nm. The derivatives **8** were measured in trifluoroacetic acid due to their low solubility. The absorption maxima were at 385 nm for the alkylated and at 414 nm for the perfluoralkylated derivatives. In contrast to the twisted OAPP (**7**), the maxima of the alkylated compounds have a smaller wavelength than the perfluoroalkylated ones. Only the alkylated derivatives displayed emission in solution and the fluorescence spectra are also shown in Figure 6a,b (dashed lines). The absorption and emission spectra of the "oxidized" form of **8c**, the target OAPP compound (**9c**) was recorded in THF due to its

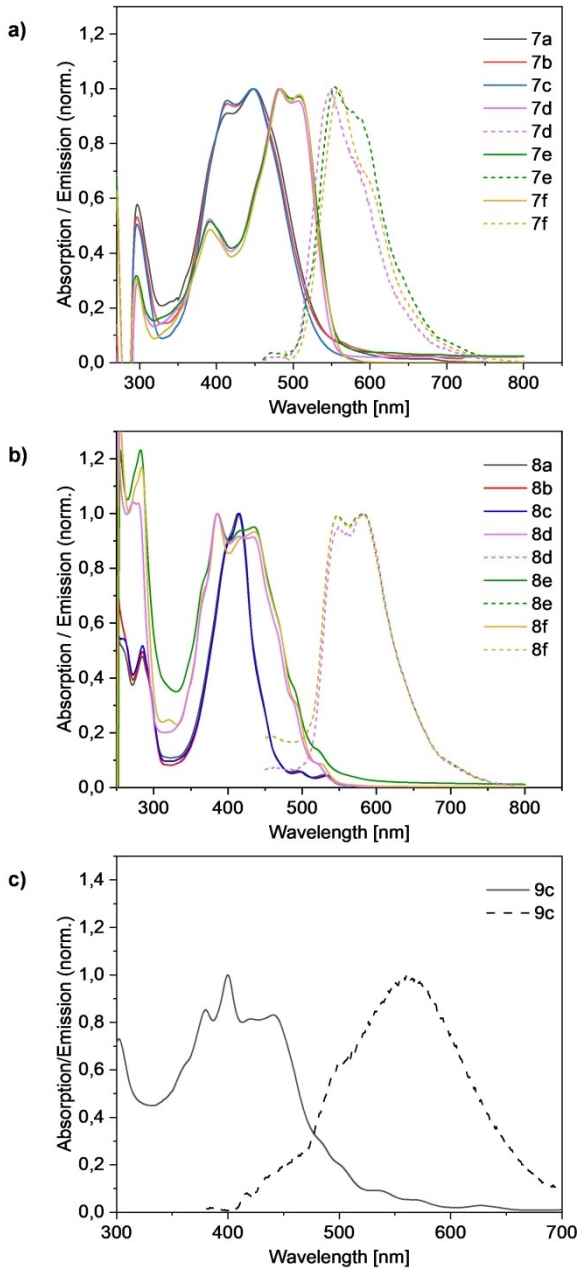

Figure 6. Absorption and emission spectra of the reduced form of the twisted OAPP **7** in THF (a), the planarized, protonated compound **8** in TFA (b) and the OAPP **9c** in THF (c).

greater solubility in such an organic solvent as compared to the hydrogen bonded reduced dihydro form. It displayed an absorption maximum at 400 nm and in contrast to the derivatives **7** and **8**, a strongly Stokes shifted emission spectrum (Figure 6c). The optical properties of compounds **7**–**9** are summarized in Table 2.

Table 2. Photophysical properties of **7**,**8**,and **9**.

	λ_{abs} [nm] (log ε)	λ_{em} [nm]	0-0-Transition [nm]	Stokes shift [cm^{-1}]
7a	449 (4.24)	/	/	/
7b	447 (4.27)	/	/	/
7c	447 (4.28)	/	/	/
7d	483 (4.23)	550	526	2522
7e	484 (4.29)	555	531	2643
7f	484 (4.34)	558	532	2740
8a	414 (4.51)	/	/	/
8b	415 (4.54)	/	/	/
8c	415 (4.53)	/	/	/
8d	386 (4.18)	582	509	8725
8e	386 (4.29)	581	505	8695
8f	386 (4.22)	581	502	8695
9c	400 (4.45)	561	477	7175

Redox properties of the OAPP derivative 9c

The redox properties of the only OAPP-derivative, which was isolable in its TAPP-analogous "oxidized" form, compound **9c** were investigated by cyclic voltammetry. Two separate one electron reduction steps were found in the cyclic voltammogram (see Figure 7). The first reduction step was found to be fully reversible, leading to the monoanionic radical species. The second reduction step exhibited quasi-reversible electron transfer characteristics and gave rise to the di-anionic OAPP. Complete decomposition of the material was observed after eight cycles, indicating the reactivity and thus lability of the OAPP redox states involved.

According to a method, which is widely employed in the literature the energy of the LUMO was estimated from the measured potential of the first reduction wave via subtraction of the potential of ferrocene (4.8 eV Fc/Fc^{+}) as reference system[79] In comparison to the corresponding TAPP (LUMO: −3.72 eV[43]) the LUMO energy is decreased by 0.7 eV due to the isosteric replacement of a further four CH-units with nitrogen.

To gain deeper insight into the electronic properties of compound **9c**, and thus generally OAPPs, various band gap-related energies of the synthetically accessible OAPP **9c** were

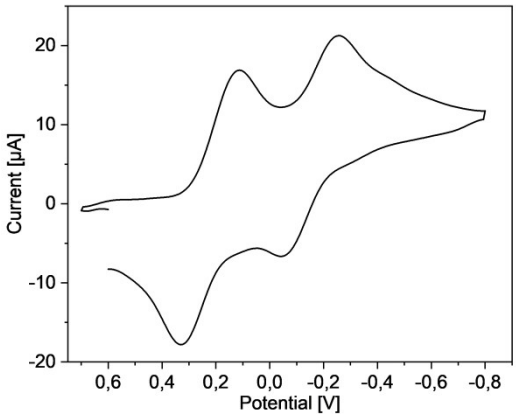

Figure 7. Cyclic voltammogram of **9c**, measured in THF, supp. electrolyte Bu_4NPF_6, reference SCE, sweep rate 50 mVs^{-1}.

modeled by DFT and TD-DFT. The validity of the results at the chosen level of theory (UB3LYP/Def2-TZVPP-GD3(BJ) with and without CPCM[80–81] as solvation model, see Supporting Information for details) could be gauged by direct comparison of the computed LUMO and optical band gap energies (E_{opt}) with the estimates based on experimental redox and photophysical data (see below). Singlet excitation energies were obtained as vertical excitations using TD-DFT, while the fundamental band gap energy E_F (or transport energy gap) was derived employing the delta self-consistent field approach (ΔSCF/DFT).[78] With the latter, the fundamental band gap (E_F) could be determined from the SCF orbital energies and the resulting SCF total energies for the neutral, oxidized, and reduced systems separately and then inserting them into the relation:

$$\Delta E_F = IP_{neut} - EA_{neut} = [E_{ox} - E_{neut}] - [E_{neut} - E_{red}]$$

Herein, IP_{neut} and EA_{neut} refer to the ionization potential and the electron affinity of the neutral compound, respectively, and $E_{ox/neut/red}$ to the total SCF energies of the oxidized, neutral, or reduced compound. The calculated fundamental gap energies were determined to be $\Delta E_F^{gas} = 5.42\ eV$ in the gas phase and $\Delta E_F^{thf} = 3.17\ eV$ in solution. The energies of the frontier orbitals and the highest occupied molecular orbital with π-character (HOPMO) were extracted directly from the single point calculations of the neutral compound as SCF-orbital energies. Here, an excellent agreement of the theoretical and experimental determined energetic LUMO position can be seen (see Table 3). A remarkably good agreement with the experiment is also noticeable when considering the calculated optical band gap (E_{opt}). Using TD-DFT, this was determined to be the first most intense singlet transition ($S_0 \rightarrow S_4$, mixing of HOMO-2→LUMO +1, HOMO-1→LUMO, and HOMO→LUMO). Three other weakly or non-dipole allowed singlet excitations are hidden under the absorption band of the $S_0 \rightarrow S_4$ excitation (for TD-DFT spectrum, see Supporting Information).

The radical anion of **9c** OAPP$^{\bullet-}$ was isolated in nearly quantitative yield by addition of one equivalent of KC_8 to a suspension of OAPP **9c** in THF.[48] The radical anion was characterized by EPR spectroscopy and revealed a *g*-factor of 2.003 (Figure 8), which is in accordance with typical delocalized organic radicals.[82] Hyperfine coupling to ^{14}N (I = 1) was not resolved for this system.[48]

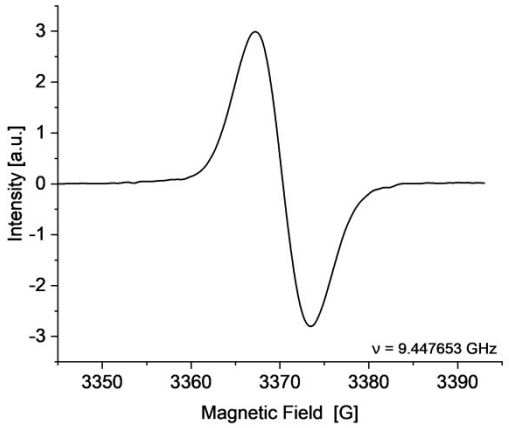

Figure 8. EPR-spectrum (THF, r.t.) of **9c**$^{\bullet-}$.

Discussion of the isosteric replacement [CH→N] in azaperopyrenes and general conclusions related to this family of poly-N-heterocyclic aromatic compounds

In this study, we extended the chemistry of azaperopyrenes (APPs), taking the previously studied TAPP as reference system, by isosteric replacement of four additional CH-units with nitrogen. In order to generalize the insight into the influence of the number and the position of the aza substitution we conclude this study by extending the computational screening to include all conceivable and distinct permutations of the isosteric [CH→N] replacement at the ortho and bay positions of the CF_3-TAPP.

Generally and notably, we found a 2D linear correlation between the number of the nitrogen atoms in the aromatic core, the position of the nitrogen atoms and the HOMO and LUMO energies (Figure 9a). The *ortho* and *bay* [CH→N] replacements independently decrease the frontier orbital energies by a defined value, more precisely each *ortho* aza substitution results in a decrease of 0.31 eV for the HOMO and 0.26 eV for the LUMO and for a *bay* substitution a reduction of 0.15 eV for the HOMO and 0.17 eV for the LUMO energy was identified (see Equation I and II). That the *ortho* isosteric replacement leads to a higher decrease of the frontier orbital energies can be traced to the larger orbital coefficients in this position (see above).

$$E_{HOMO} = (-6.80 - 0.31o - 0.15b)\ eV \quad (1)$$

$$E_{LUMO} = (-3.82 - 0.26o - 0.17b)\ eV \quad (2)$$

Table 3. Electronical properties of **9c** according to DFT calculations and CV and UV/Vis experiments.

Solvent model	EA[a] [eV]	HOMO[b] [eV]	HOPMO[b] [eV]	LUMO[b] [eV]	E_F [a] [eV]	E_{opt} [c] [eV]	LUMO (CV)[d] [eV]	E_{opt} [d] (UV/Vis) [eV]
Gas	3.76	−8.01	−8.23	−4.90	5.42	3.17	–	–
thf	4.54	−7.74	−7.80	−4.44	3.17	3.11	−4.47	3.10

[a] Properties were calculated using the ΔSCF/DFT approach.[78] [b] Properties were calculated as the SCF-orbital energies of the neutral compound. [c] The optical band gap (E_{opt}) was obtained as the first singlet state with the largest oscillator strength via TD-DFT. [d] Values were determined experimentally. HOPMO: highest occupied molecular orbital with π-character, E_F: fundamental band gap, E_{opt}: optical band gap.

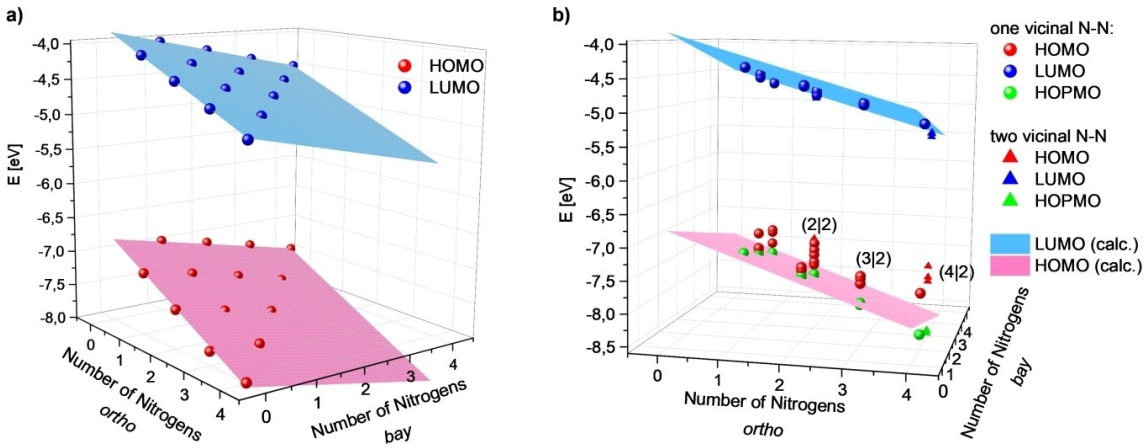

Figure 9. Left: Correlation between the frontier orbital energies of azaperopyrenes, which do not possess a vicinal N–N arrangement, and the number of *ortho* and *bay* aza substitutions. Right: Comparison of HOMO, HOPMO and LUMO energies for azaperopyrenes which have at least one N–N bond.

(o = number of nitrogen in the *ortho* position, b = number of nitrogen in the *bay* position)

For constitutional isomers with a vicinal N–N arrangement, the HOMO energies deviate from the idealized Equation I, and are higher than expected (Figure 9b). This result arises from the fact that in these isomers the HOMO has σ-symmetry within the aromatic plane and significant lone pair character, mainly localized at the vicinal nitrogen atoms (Figure 10b). Therefore, the resulting Pauli repulsion of the N-lone pairs increases the energy of this type of HOMO.

However, if one considers the highest occupied molecular orbital with π–character (HOPMO) for these constitutional isomers, instead of the lone pair based HOMOs, a good agreement (Figure 9b) with the linearly approximated HOMO energies in Equation I is generally found. Notably, for the case of *two pairs of vicinal* nitrogen atoms in one molecule, the HOPMO was in accordance to the expected HOMO energies for the derivatives with two *bay* and two *ortho* aza substitutions. On the other hand, for higher numbers of nitrogen atoms (e.g., four *ortho* + two *bay*) the HOPMO energies are lower than expected. Generally the deviation of the LUMO energies of the vicinally substituted isomers compared to the other isomers is small and insignificant given the DFT method employed.

In summary, the peropyrene structure allows the specific variation of the frontier orbital energies for a certain application by adding nitrogen atoms into the aromatic core. This in principle allows the tuning of the LUMO energy close to the work function of gold, which is important for the use of the azaperopyrenes as *n*-semiconducting materials, without adding substituents to the aromatic core. In the development of nitrogen rich N-heteropolycycles based on the peropyrene core structure the OAPP **9c** reported and characterized in this work represents an extreme case as electron acceptors. In terms of [CH→N] replacements current and future work in our lab will therefore address the chemical space between the TAPPs and the OAPPS.

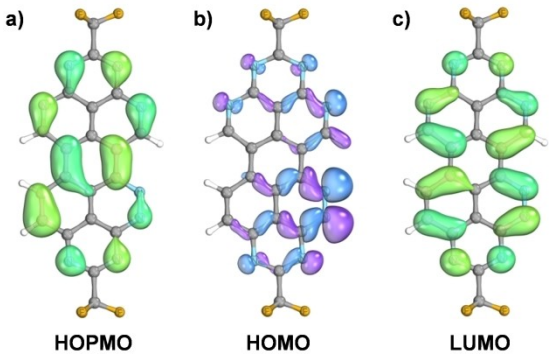

Figure 10. Visualization (IBOview[83], Threshold = 78) of the HOPMO (a), HOMO (b) and LUMO (c) of an octaazaperopyrene with a N–N bond (B3LYP/Def2-TZVPP-GD3(BJ) level of theory).

Experimental Section

General Information

All chemicals and solvents were purchased from commercial suppliers and used without further purification. Solvents were dried according to standard procedures. Deuterated solvents were bought from Euriso Top or Sigma Aldrich and used as received. The ^{1}H, ^{13}C and ^{19}F spectra were recorded with Bruker AVANCE 400 and 600II spectrometers and are referenced to the residual signal of the used deuterated solvents (^{1}H: $CDCl_3$: 7.26 ppm, THF-d_8: 1.72 ppm/3.58 ppm, DMSO-d_6:2.50 ppm) and ^{13}C: $CDCl_3$: 77.16 ppm, THF-d_8: 67.21 ppm/25.31 ppm, DMSO-d_6: 39.52 ppm).[84] Chemical shifts are given in ppm and coupling constants in Hz. The following abbreviations were used to describe the multiplicities: s = singlet, d = doublet, t = triplet, q = quartet, quint = quintet, m = multiplet. The mass spectra were recorded by the department of the organic Chemistry of the University of Heidelberg under the direction of Dr. J. Gross. EI spectra were measured on a JEOL JMS 700 spectrometer, ESI spectra on a Bruker ApexQe hybrid 9.4 T FT-ICR (also for MALDI spectra) or a Finnigan LCQ spectrometer. The absorption spectra were recorded on a Cary 5000 UV/Vis- spectrometer and were baseline and solvent corrected. The Fluorescence spectra were recorded on a Varian Cary Eclipse Fluorescence spectrophotometer.

The Fluorescence Yields (Φ) were conducted on a JASCO spectrofluorometer FP-8500 equipped with an ILF-835 | 100 mm integrating sphere. Cyclic voltammetry spectra were measured on a EG&G Princeton Applied Research potentiostat model 263 A using a three-electrode single-component cell under inert atmosphere. A platinum disk was used as working electrode, platinum wire as a counter electrode and a saturated calomel electrode as a reference electrode. As internal reference ferrocene was used in all cases. Measurements were carried out in a 0.1 M tetrabutylammonium hexafluorophosphate solution in anhydrous THF und exclusion of oxygen. X-ray analyses were performed by Prof. Dr. H. Wadepohl in the structure-analytical laboratory of the Department of Inorganic Chemistry at the University of Heidelberg with a Bruker AXS Smart 1000 diffractometer or an Agilent Supernova E diffractometer. The obtained structures were resolved by Prof. Dr. H. Wadepohl. Infrared spectra were measured on a Bruker FT IR with a Germanium ATR crystal. Unless otherwise stated, all preparative work was performed in an inert gas atmosphere in standard Schlenk glassware, which was flame-dried.

General Procedure 1

3,4,9,10,-tetraamino-1,6,7,12-tetrachloro-2,5,8,11-tetraazaperylene (1.00 eq.) was dissolved in 1,4-dioxane. Triethylamine (3.00 eq.) and acyl chloride (5.50 eq.) were added and the reaction solution was stirred at 100 °C for 7 d. The reaction mixture was allowed to cool down to r.t. and the resulting precipitate was filtered. The residue was washed with water and the crude product was recrystallized from ethanol to yield the product as an orange solid.

General Procedure 2

Formic acid (36.0 eq.) was dissolved in DMF, triethylamine (36.0 eq.) was added dropwise and stirred at r.t. for 30 min. $[Pd(PPh_3)_4]$ (20 mol%), the corresponding aryl chloride (1.00 eq.) were added and the reaction mixture was stirred at 80 °C for 2 d. The reaction mixture was allowed to cool down to r.t. and poured onto water. The resulting precipitate was filtered and washed with H_2O, acetone and THF.

2,7-Naphthyridine-1,3,6,8-tetraol (2)[71]

Diethyl-1,3-acetonedicarboxylate (35.9 ml, 198 mmol, 1.00 equiv.) was dissolved in 350 ml ethanol, malononitrile (15.7 g, 237 mmol, 1.20 equiv.) and diethyl amine (2.7 ml, 26 mmol, 0.13 equiv.) were added and the reaction mixture was stirred at r.t. for 2d. The solvent was removed under reduced pressure, the residue was dissolved in 70% H_2SO_4 (300 ml) and stirred at 140 °C for 20 min. The reaction mixture was allowed to cool down to r.t. and poured onto water (400 ml). The resulting precipitate was filtered and washed with H_2O (3x 200 ml). The remaining water was removed by azeotropic distillation with benzene to yield **2** as beige solid (47.0 g, 241 mmol, 61%).^{1}H NMR (600.13 MHz, DMSO-d_6, 295 K): δ [ppm] = 11.37 (s, 2H), 5.76 (s, 2H), 5.50 (s, 2H).^{13}C NMR (150.90 MHz, DMSO-d_6, 295 K): δ [ppm] = 169.6, 169.3, 165.6, 163.6, 162.5, 151.3, 148.8, 104.7, 89.1, 35.7. HRMS (EI$^+$): calcd. for $C_8H_6N_2O_4$ $(M)^+$: 194.0322; found: 194.0319. Analytics are in agreement with previously reported data.[71]

4,10-Dihydroxy-5,11-dihydro-2,5,8,11-tetraazaperylen-e1,3,6,7,9,12-hexaone (3)[73]

1,3,6,8-tetrahydroxy-2,7-naphthyridine (10.0 g, 51.5 mmol, 1.00 equiv.) was suspended in 210 ml 0.25 M $NaOH_{(aq)}$ and H_2O_2 (6.4 ml, 206 mmol, 4.00 eq.) was added over a period of 4 h. The reaction mixture was stirred for 16 h at room temperature and the resulting precipitate was filtered. The residue was washed with 1 l H_2O to yield **3** as a blue solid (8.11 g, 21.2 mmol, 82%). ^{13}C NMR (150.90 MHz, D_2SO_4, 295 K): δ [ppm] = 167.3, 162.3, 136.8, 124.8, 88.4. HRMS (ESI$^-$): calcd. for $C_{16}H_7N_4O_8$ $(M–H)^-$: 381.01129; found: 381.0091. Analytics are in agreement with previously reported data[73]

1,3,4,6,7,9,10,12-Octachloro-2,5,8,11-tetraazaperylene (4)[74]

4,10-dihydroxy-5,11-dihydro-2,5,8,11-tetraazaperylene1,3,6,7,9,12-hexaone (2.50 g, 6.54 mmol, 1.00 equiv.) and PCl_5 (25.0 g, 120 mmol, 18.4 equiv.) were dissolved in $POCl_3$ (25 ml, 268 mmol, 41.0 equiv.). The reaction mixture was stirred at 160 °C for 2 d. The reaction mixture was poured onto ice and the resulting precipitate was filtered. The residue was washed with 500 ml H_2O to yield **4** as an orange solid (2.10 g, 3.95 mmol, 83%). ^{13}C NMR (150.90 MHz, nitrobenzene-d_5, 295 K): δ [ppm] = 148.3, 146.5, 144.6, 117.1, 116.9. HRMS (MALDI$^-$): calcd. for $C_{16}Cl_8N_4$ $(M)^-$: 527.7637; found: 527.7642.

1,6,7,12-Tetrachloro-N^3,N^4,N^9,N^{10}-tetrakis(4-methoxybenzyl)dipyrido[3,4,5-de:3′,4′,5′-gh][2,9]phenanthrolinline-3,4,9,10-tetraamine(5)

1,3,4,6,7,9,10,12-octachloro-2,5,8,11-tetraazaperylene (10.0 g, 18.8 mmol, 1.00 eq.) was dissolved in 150 ml o-xylene. 4-methoxy benzylamine (61.0 ml, 470 mmol, 25.0 eq.) was added and the reaction mixture was stirred at 150 °C for 3 h. The solution was allowed to cool to r.t. and poured onto 400 ml methanol. The resulting precipitate was filtered, washed with 400 ml H_2O and 400 ml methanol. Solvent residuals were removed under reduced pressure and the product was obtained as a red orange solid (13.5 g, 14.4 mmol, 77%).^{1}H NMR (600.13 MHz, $CDCl_3$, 295 K): δ [ppm] = 7.14 (d, $^3J_{H\text{-}H}$ = 7.95 Hz, 8H), 6.81 (d, $^3J_{H\text{-}H}$ = 8.30 Hz, 8H), 5.79 (s, 4H, NH), 4.50–4.43 (m, 8H), 3.81 (s, 12H). ^{13}C NMR (150.90 MHz, $CDCl_3$, 295 K): δ [ppm] = 159.2, 152.6, 144.6, 144.0, 129.7, 129.4, 125.8, 114.2, 98.5, 55.3, 46.4. HRMS (MALDI$^+$): calcd. for $C_{48}H_{40}Cl_4N_4O_4$ $(M)^+$: 932.1921; found: 932.1941.

3,4,9,10,–Tetraamino-1,6,7,12-tetrachloro-2,5,8,11-tetraazaperylene (6)

Compound **5** (13.5 g, 14.4 mmol, 1.00 equiv.) was dissolved in 100 ml TFA and stirred at 80 °C for 16 h. The solution was allowed to cool to r.t. and the solvent was removed under reduced pressure. The residue was dissolved in 50 ml H_2O and neutralized with K_2CO_3. The resulting precipitate was filtered, washed with 400 ml H_2O, methanol (3x 200 ml), acetone (3x 200 ml) and *n*-pentane (2x 200 ml). The product was obtained as a red brown solid (5.10 g, 11.2 mmol, 78%).^{1}H NMR (600.13 MHz, DMSO-d_6, 295 K): δ [ppm] = 7.25 (s, 8H). ^{13}C NMR (150.90 MHz, DMSO-d_6, 295 K): δ [ppm] = 154.5, 145.5, 144.8, 107.7, 96.8. HRMS (MALDI$^+$): calcd. for $C_{16}H_8Cl_4N_8$ $(M)^+$: 451.9621; found: 451.9625.

Compound 7 a

According to GP1 3,4,9,10,-tetraamino-1,6,7,12-tetrachloro-2,5,8,11-tetraazaperylene (750 mg, 1.65 mmol, 1.00 eq.) was dissolved in 20 ml 1,4-dioxane. Triethylamine (690 µl, 4.95 mmol 3.00 eq.) and TFAA (1.26 ml, 9.08 mmol, 5.50 eq.) were added and the reaction solution was stirred at 60 °C for 7 d. The reaction mixture was allowed to cool down to r.t. and the resulting precipitate was filtered. The residue was washed with water and the crude product

was recrystallized from ethanol to yield the product as an orange solid (532 mg, 872 μmol, 53%). ^{1}H NMR (600.13 MHz, DMSO-d_6, 363 K): δ [ppm] = 5.61 (bs, 2H). ^{13}C NMR (150.90 MHz, DMSO-d_6, 353 K): δ [ppm] = 158.4, 152.2, 146.0, 114.4, 110.3. ^{19}F NMR (379.27 MHz, DMSO-d_6, 295 K): δ [ppm] = −70.6 (s, 6F). HRMS (MALDI$^-$): calcd. for $C_{20}Cl_4F_6N_8$ $(M)^-$ (oxidized form): 605.8910; found: 605.8910.

Compound 7 b

According to GP1 3,4,9,10,–tetraamino-1,6,7,12-tetrachloro-2,5,8,11-tetraazaperylene (750 mg, 1.65 mmol, 1.00 eq.) was dissolved in 20 ml 1,4-dioxane. Triethylamine (690 μl, 4.95 mmol 3.00 eq.) and pentafluoropropionic anhydride (1.79 ml, 9.08 mmol, 5.50 eq.) were added and the reaction solution was stirred at 100 °C for 7 d. The reaction mixture was allowed to cool down to r.t. and the resulting precipitate was filtered. The residue was washed with water and the crude product was recrystallized from ethanol to yield the product as an orange solid (552 mg, 777 μmol, 47%). ^{1}H NMR (600.13 MHz, DMSO-d_6, 353 K): δ [ppm] = 5.37 (bs, 2H). ^{13}C NMR (150.90 MHz, DMSO-d_6, 353 K): δ [ppm] = 158.2, 157.2, 152.1, 145.6, 114.5, 110.2. ^{19}F NMR (379.27 MHz, DMSO-d_6, 295 K): δ [ppm] = −81.3 (s, 6F), −117.2 (q, $^{3}J_{F\text{-}F}$ = 105.3 Hz, 4F). HRMS (MALDI$^-$): calcd. for $C_{22}Cl_4F_{10}N_8$ $(M)^-$ (oxidized form): 705.8846; found: 705.8847.

Compound 7 c

According to GP1 3,4,9,10,–tetraamino-1,6,7,12-tetrachloro-2,5,8,11-tetraazaperylene (1.00 g, 2.20 mmol, 1.00 eq.) was dissolved in 30 ml 1,4-dioxane. Triethylamine (920 μl, 6.61 mmol 3.00 eq.) and perfluorobutyryl chloride (1.80 ml, 12.1 mmol, 5.50 eq.) were added and the reaction solution was stirred at 100 °C for 7 d. The reaction mixture was allowed to cool down to r.t. and the resulting precipitate was filtered. The residue was washed with water (2x 50 ml) and the crude product was recrystallized from ethanol to yield the product as an orange solid (906 mg, 1.12 mmol, 51%). ^{1}H NMR (600.13 MHz, DMSO-d_6, 350 K): δ [ppm] = 6.83 (bs, 2H). ^{13}C NMR (150.90 MHz, DMSO-d_6, 353 K): δ [ppm] = 158.5, 157.6, 152.3, 145.7, 114.5, 110.2. ^{19}F NMR (379.27 MHz, DMSO-d_6, 295 K): δ [ppm] = −79.8 (t, $^{3}J_{F\text{-}F}$ = 8.60 Hz, 6F), −115.5 (q, $^{3}J_{F\text{-}F}$ = 252.8 Hz, 4F), −125.7 (s, 4F). HRMS (MALDI$^-$): calcd. for $C_{24}Cl_4F_{14}N_8$ $(M)^-$ (oxidized form): 807.8752; found: 807.8758.

Compound 7 d

According to GP1 3,4,9,10,–tetraamino-1,6,7,12-tetrachloro-2,5,8,11-tetraazaperylene (300 mg, 661 μmol, 1.00 eq.) was dissolved in 10 ml 1,4-dioxane. Triethylamine (275 μl, 1.98 mmol 3.00 eq.) and acetyl chloride (260 μl, 3.63 mmol, 5.50 eq.) were added and the reaction solution was stirred at 100 °C for 7 d. The reaction mixture was allowed to cool down to r.t. and the resulting precipitate was filtered. The residue was washed with water (2x 50 ml), methanol (2x 20 ml) and the crude product was recrystallized from ethanol to yield the product as an orange red solid (183 mg, 364 μmol, 55%).^{1}H NMR (600.13 MHz, DMSO-d_6, 295 K): δ [ppm] = 2.37 (s, 6H). ^{13}C NMR (150.90 MHz, DMSO-d_6, 353 K): δ [ppm] = 161.8, 154.0, 149.9, 148.1, 114.4, 107.6, 22.4. HRMS (MALDI$^+$): calcd. for $C_{20}H_8Cl_4N_8$ $(M)^+$ (oxidized form): 499.9621; found: 499.9616.

Compound 7 e

According to GP1 3,4,9,10,–tetraamino-1,6,7,12-tetrachloro-2,5,8,11-tetraazaperylene (750 mg, 1.65 mmol, 1.00 eq.) was dissolved in 15 ml 1,4-dioxane. Triethylamine (690 μl, 4.95 mmol 3.00 eq.) and butyryl chloride (940 μl, 9.08 mmol, 5.50 eq.) were added and the reaction solution was stirred at 100 °C for 7 d. The reaction mixture was allowed to cool down to r.t. and the resulting precipitate was filtered. The residue was washed with water (2x 50 ml) and the crude product was recrystallized from ethanol to yield the product as an orange solid (556 mg, 996 μmol, 60%).^{1}H NMR (600.13 MHz, THF-d_8, 295 K): δ [ppm] = 11.82 (bs, 2H), 2.60 (t, $^{3}J_{H\text{-}H}$ = 7.60 Hz 4H), 1.86 (sext, $^{3}J_{H\text{-}H}$ = 7.43 Hz 4H), 1.04 (t, $^{3}J_{H\text{-}H}$ = 7.35 Hz 4H). ^{13}C NMR (150.90 MHz, DMSO-d_6, 353 K): δ [ppm] = 164.8, 154.1, 150.0, 148.2, 114.4, 107.8, 37.2, 20.4, 13.7. HRMS (MALDI$^+$): calcd. for $C_{24}H_{16}Cl_4N_8$ $(M)^+$ (oxidized form): 556.0247; found: 556.0241.

Compound 7 f

According to GP1 3,4,9,10, -tetraamino-1,6,7,12-tetrachloro-2,5,8,11-tetraazaperylene (500 mg, 1.10 mmol, 1.00 eq.) was dissolved in 15 ml 1,4-dioxane. Triethylamine (460 μl, 3.30 mmol 3.00 eq.) and 3,3-dimethylbutanoyl chloride (841 μl, 6.06 mmol, 5.50 eq.) were added and the reaction solution was stirred at 100 °C for 7 d. The reaction mixture was allowed to cool down to r.t. and the resulting precipitate was filtered. The residue was washed with water (3x 50 ml) and the crude product was recrystallized from ethanol to yield the product as an orange solid (334 mg, 544 μmol, 49%).^{1}H NMR (399.89 MHz, D_2SO_4-d_2, 295 K): δ [ppm] = 3.14 (s, 4H), 1.20 (s, 18H). ^{13}C NMR (150.90 MHz, D_2SO_4-d_2, 295 K): δ [ppm] = 169.5, 149.5, 147.4, 145.8, 116.2, 105.7, 48.3, 35.6, 28.2.HRMS (MALDI$^+$): calcd. for $C_{28}H_{24}Cl_4N_8$ $(M)^+$ (oxidized form): 612.0872; found: 612.0871.

Compound 8 a

According to GP2 formic acid (1.00 ml, 26.6 mmol, 36.0 eq.) was dissolved in 15 ml DMF, triethylamine (3.70 ml, 26.6 mmol, 36.0 eq.) was added dropwise and stirred at r.t. for 30 min. [Pd(PPh_3)$_4$] (170 mg, 148 μmol, 20 mol%), compound **7 a** (450 mg, 738 μmol, 1.00 eq.) were added and the reaction mixture was stirred at 80 °C for 2 d. The reaction mixture was allowed to cool down to r.t. and poured onto 100 ml water. The resulting precipitate was filtered and washed with H_2O (3x 50 ml), acetone (2x 30 ml) and THF (2x 30 ml) to yield the product as an orange red solid (296 mg, 738 μmol, 85%). ^{1}H NMR (600.13 MHz, D_2SO_4-d_2, 295 K): δ [ppm] = 8.49 (s, 4H). ^{13}C NMR (150.90 MHz, D_2SO_4-d_2, 295 K): δ [ppm] = 152.1 (q, $^{2}J_{C\text{-}F}$ = 43.9 Hz), 150.0, 145.4, 138.3 (q, $^{4}J_{C\text{-}F}$ = 16.1 Hz), 120.1, 115.6 (q, $^{1}J_{C\text{-}F}$ 278.9 Hz), 113.7. ^{19}F NMR (379.27 MHz, D_2SO_4-d_2, 295 K): δ [ppm] = −71.3 (s, 6F). HRMS (MALDI$^-$): calcd. for $C_{20}H_4F_6N_8$ $(M)^-$ (oxidized form): 470.0469; found: 470.0482.

Compound 8 b

According to GP2 formic acid (956 μl, 25.4 mmol, 36.0 eq.) was dissolved in 15 ml DMF, triethylamine (3.53 ml, 25.4 mmol, 36.0 eq.) was added dropwise and stirred at r.t. for 30 min. [Pd(PPh_3)$_4$] (163 mg, 141 μmol, 20 mol%), compound **7 b** (500 mg, 704 μmol, 1.00 eq.) were added and the reaction mixture was stirred at 80 °C for 2 d. The reaction mixture was allowed to cool down to r.t. and poured onto 100 ml water. The resulting precipitate was filtered and washed with H_2O (3x 50 ml), acetone (2x 30 ml) and THF (2x 30 ml) to yield the product as an orange red solid (216 mg, 377 μmol, 54%). ^{1}H NMR (600.13 MHz, D_2SO_4-d_2, 295 K): δ [ppm] = 8.74 (s, 4H). ^{13}C NMR (150.90 MHz, D_2SO_4-d_2, 295 K): δ [ppm] = 149.9, 145.5, 138.4 (q, $^{4}J_{C\text{-}F}$ = 16.7 Hz), 120.2, 113.7. ^{13}C signals of the N–C–N– and perfluorinated alkyl groups could not be detected due to coupling to fluorine groups.^{19}F NMR (379.27 MHz, D_2SO_4-d_2, 295 K): δ [ppm] = −82.0 (s, 6F), −119.8 (s, 24). HRMS (MALDI$^-$): calcd. for $C_{22}H_4F_{10}N_8$ $(M)^-$ (oxidized form): 570.0402; found: 570.0412.

Compound 8c

According to GP2 formic acid (838 µl, 22.2 mmol, 36.0 eq.) was dissolved in 15 ml DMF, triethylamine (3.10 ml, 22.2 mmol, 36.0 eq.) was added dropwise and stirred at r.t. for 30 min. [$Pd(PPh_3)_4$] (143 mg, 123 µmol, 20 mol%), compound **7c** (500 mg, 617 µmol, 1.00 eq.) were added and the reaction mixture was stirred at 80 °C for 2 d. The reaction mixture was allowed to cool down to r.t. and poured onto 150 ml water. The resulting precipitate was filtered and washed with H_2O (3x 50 ml), acetone (2x 30 ml) and THF (2x 30 ml) to yield the product as an orange red solid (328 mg, 617 µmol, 79%). ^{1}H NMR (600.13 MHz, D_2SO_4-d_2, 295 K): δ [ppm] = 8.72 (s, 4H). ^{13}C NMR (150.90 MHz, D_2SO_4-d_2, 295 K): δ [ppm] = 149.9, 145.5, 138.4 (q, $^4J_{C\text{-}F}$ = 17.2 Hz), 120.2, 113.7.^{13}C signals of the N–C-N- and perfluorinated alkyl groups could not be detected due to coupling to fluorine groups.^{19}F NMR (379.27 MHz, D_2SO_4-d_2, 295 K): δ [ppm] = −80.1 (t, $^3J_{F\text{-}F}$ = 8.87 Hz, 6F), −117.2 (s, 4F), −124.8 (s, 4F). HRMS (MALDI$^-$): calcd. for $C_{22}H_4F_{10}N_8$ $(M)^-$ (oxidized form): 670.0341; found: 670.0342.

Compound 8d

According to GP2 formic acid (1.11 ml, 29.3 mmol, 36.0 eq.) was dissolved in 15 ml DMF, triethylamine (4.09 ml, 29.3 mmol, 36.0 eq.) was added dropwise and stirred at r.t. for 30 min. [$Pd(PPh_3)_4$] (188 mg, 163 µmol, 20 mol%), compound **7d** (409 mg, 815 µmol, 1.00 eq.) were added and the reaction mixture was stirred at 80 °C for 2 d. The reaction mixture was allowed to cool down to r.t. and poured onto 150 ml water. The resulting precipitate was filtered and washed with H_2O (3x 50 ml), acetone (2x 30 ml) and THF (2x 30 ml) to yield the product as an orange red solid (101 mg, 277 µmol, 34%). ^{1}H NMR (600.13 MHz, D_2SO_4-d_2, 295 K): δ [ppm] = 8.43 (s, 4H), 2.58 (s, 6H). ^{13}C NMR (150.90 MHz, D_2SO_4-d_2, 295 K): δ [ppm] = 168.0, 148.3, 144.2, 137.2, 118.4, 111.1. HRMS (MALDI$^+$): calcd. for $C_{20}H_{13}N_8$ $(M)^+$: 365.1258; found: 365.1269.

Compound 8e

According to GP2 formic acid (608 µl, 16.1 mmol, 36.0 eq.) was dissolved in 10 ml DMF, triethylamine (2.25 ml, 16.1 mmol, 36.0 eq.) was added dropwise and stirred at r.t. for 30 min. [$Pd(PPh_3)_4$] (104 mg, 89.6 µmol, 20 mol%), compound **7e** (250 mg, 448 µmol, 1.00 eq.) were added and the reaction mixture was stirred at 80 °C for 2 d. The reaction mixture was allowed to cool down to r.t. and poured onto 100 ml water. The resulting precipitate was filtered and washed with H_2O (3x 50 ml), acetone (2x 30 ml) and THF (2x 30 ml) to yield the product as an orange red solid (78.0 mg, 186 µmol, 41%). ^{1}H NMR (600.13 MHz, D_2SO_4-d_2, 295 K): δ [ppm] = 8.37 (s, 4H), 2.66 (s, 4H), 1.54 (quint., $^3J_{H\text{-}H}$ = 6.60 Hz 4H), 0.66 (t, $^3J_{H\text{-}H}$ = 6.36 Hz 6H). ^{13}C NMR (150.90 MHz, D_2SO_4-d_2, 295 K): δ [ppm] = 171.0, 148.4, 144.4, 137.1, 118.3, 111.2, 36.7, 19.9, 12.2. HRMS (MALDI$^+$): calcd. for $C_{24}H_{20}N_8$ $(M+H)^+$: 421.1884; found: 421.1889.

Compound 8f

According to GP2 formic acid (553 µl, 14.7 mmol, 36.0 eq.) was dissolved in 10 ml DMF, triethylamine (2.04 ml, 14.7 mmol, 36.0 eq.) was added dropwise and stirred at r.t. for 30 min. [$Pd(PPh_3)_4$] (94.1 mg, 81.4 µmol, 20 mol%), compound **7f** (250 mg, 407 µmol, 1.00 eq.) were added and the reaction mixture was stirred at 80 °C for 2 d. The reaction mixture was allowed to cool down to r.t. and poured onto 100 ml water. The resulting precipitate was filtered and washed with H_2O (3x 50 ml), acetone (2x 30 ml) and THF (2x 30 ml) to yield the product as an orange red solid (112 mg, 235 µmol, 58%). ^{1}H NMR (600.13 MHz, D_2SO_4-d_2, 295 K): δ [ppm] = 8.37 (s, 4H), 2.57 (s, 4H), 0.74 (s, 18H). ^{13}C NMR (150.90 MHz, D_2SO_4-d_2, 295 K): δ [ppm] = 169.2, 148.7, 144.6, 137.0, 118.1, 111.3, 49.3, 34.7, 28.3. HRMS (EI$^+$): calcd. for $C_{28}H_{28}N_8$ $(M)^+$: 476.24314; found: 476.24122.

Compound 9c

Compound **8c** (40.0 mg, 59.5 µmol, 1.00 eq.) and MnO_2 (93.1 mg, 1.07 mmol, 18.0 eq) were suspended in 5 ml THF and the reaction mixture was stirred at r.t. for 2 h. The reaction mixture was filtered over Celite and the solvent was removed under reduced pressure to give the product as a yellow solid (35.0 mg, 52.2 µmol, 88%). ^{1}H NMR (399.89 MHz, THF-d_8, 295 K): δ [ppm] = 11.86 (s, 4H). ^{13}C NMR (150.90 MHz, THF-d_8, 295 K): δ [ppm] = 158.6, 158.2, 123.8, 120.7, 103.4. ^{13}C signals of the N–C–N– and perfluorinated alkyl groups could not be detected due to coupling to fluorine groups.^{19}F NMR (379.27 MHz, D_2SO_4-d_2, 295 K): δ [ppm] = −81.1 (t, $^3J_{F\text{-}F}$ = 9.22 Hz, 6F), −113.6 (q, $^3J_{F\text{-}F}$ = 9.23 Hz, 4F), −126.0 (s, 4F). HRMS (MALDI$^-$): calcd. for $C_{22}H_4F_{10}N_8$ $(M)^-$: 670.0341; found: 670.0342.

Deposition Numbers

Deposition Number(s) 2130535 (for **4**), 2130536 (for **7a**), 2130537 (for **8a**) and 2130538 (for **8e**) contain(s) the supplementary crystallographic data for this paper. These data are provided free of charge by the joint Cambridge Crystallographic Data Centre and Fachinformationszentrum Karlsruhe "http://www.ccdc.cam.ac.uk/structures"Access Structures service.

Acknowledgements

The authors acknowledge support by the state of Baden-Württemberg through bwHPC and the German Research Foundation (DFG) through no. INST 40/467-1 FUGG (Just cluster). Open Access funding enabled and organized by Projekt DEAL.

Conflict of Interest

The authors declare no conflict of interest.

Data Availability Statement

Research data are not shared.

Keywords: azaperylenes · DFT calculations · N-heteropolycycles · organic dyes · redox reactions

[1] J.-F. Morin, *J. Mater. Chem. C* **2017**, *5*, 12298–12307.
[2] A. Nowak-Król, F. Würthner, *Org. Chem. Front.* **2019**, *6*, 1272–1318.
[3] Q. Miao, *Adv. Mater.* **2014**, *26*, 5541–5549.
[4] U. H. F. Bunz, *Acc. Chem. Res.* **2015**, *48*, 1676–1686.
[5] U. H. F. Bunz, J. U. Engelhart, *Chem. Eur. J.* **2016**, *22*, 4680–4689.
[6] U. H. F. Bunz, J. Freudenberg, *Acc. Chem. Res.* **2019**, *52*, 1575–1587.

[7] A. Borissov, Y. K. Maurya, L. Moshniaha, W.-S. Wong, M. Żyła-Karwowska, M. Stępień, *Chem. Rev.* **2021**.
[8] M. Gsänger, D. Bialas, L. Huang, M. Stolte, F. Würthner, *Adv. Mater.* **2016**, *28*, 3615–3645.
[9] M. J. Robb, S.-Y. Ku, F. G. Brunetti, C. J. Hawker, *J. Polym. Sci. Part A* **2013**, *51*, 1263–1271.
[10] J. Zaumseil, H. Sirringhaus, *Chem. Rev.* **2007**, *107*, 1296–1323.
[11] H. Klauk, *Chem. Soc. Rev.* **2010**, *39*, 2643–2666.
[12] A. F. Paterson, S. Singh, K. J. Fallon, T. Hodsden, Y. Han, B. C. Schroeder, H. Bronstein, M. Heeney, I. McCulloch, T. D. Anthopoulos, *Adv. Mater.* **2018**, *30*, 1801079.
[13] J. T. E. Quinn, J. Zhu, X. Li, J. Wang, Y. Li, *J. Mater. Chem. C* **2017**, *5*, 8654–8681.
[14] J. E. Anthony, *Chem. Rev.* **2006**, *106*, 5028–5048.
[15] M. Winkler, K. N. Houk, *J. Am. Chem. Soc.* **2007**, *129*, 1805–1815.
[16] H.-Y. Chen, I. Chao, *ChemPhysChem* **2006**, *7*, 2003–2007.
[17] U. H. F. Bunz, J. U. Engelhart, B. D. Lindner, M. Schaffroth, *Angew. Chem. Int. Ed.* **2013**, *52*, 3810–3821; *Angew. Chem.* **2013**, *125*, 3898–3910.
[18] U. H. F. Bunz, *Chem. Eur. J.* **2009**, *15*, 6780–6789.
[19] S. Miao, A. L. Appleton, N. Berger, S. Barlow, S. R. Marder, K. I. Hardcastle, U. H. F. Bunz, *Chem. Eur. J.* **2009**, *15*, 4990–4993.
[20] X.-D. Tang, Y. Liao, H. Geng, Z.-G. Shuai, *J. Mater. Chem.* **2012**, *22*, 18181–18191.
[21] O. Hinsberg, *Justus Liebigs Ann. Chem.* **1901**, *319*, 257–286.
[22] O. Fischer, E. Hepp, *Chem. Ber.* **1890**, *23*, 2789–2793.
[23] E. Leete, O. Ekechukwu, P. Delvigs, *J. Org. Chem.* **1966**, *31*, 3734–3739.
[24] F. Kummer, H. Zimmermann, *Ber. Bunsen-Ges. Phys. Chem.* **1967**, *71*, 1119-+.
[25] G. M. Badger, R. Pettit, *J. Chem. Soc.* **1951**, 3211–3215.
[26] G. Xie, M. Hauschild, H. Hoffmann, L. Ahrens, F. Rominger, M. Borkowski, T. Marszalek, J. Freudenberg, M. Kivala, U. H. F. Bunz, *Chem. Eur. J.* **2020**, *26*, 799–803.
[27] S. Miao, M. D. Smith, U. H. F. Bunz, *Org. Lett.* **2006**, *8*, 757–760.
[28] M. Märken, B. D. Lindner, A. L. Appleton, F. Rominger, U. H. F. Bunz, *Pure Appl. Chem.* **2014**, *86*, 483–488.
[29] O. Tverskoy, F. Rominger, A. Peters, H.-J. Himmel, U. H. F. Bunz, *Angew. Chem. Int. Ed.* **2011**, *50*, 3557–3560; *Angew. Chem.* **2011**, *123*, 3619–3622.
[30] A. L. Appleton, S. M. Brombosz, S. Barlow, J. S. Sears, J.-L. Bredas, S. R. Marder, U. H. F. Bunz, *Nat. Commun.* **2010**, *1*, 91.
[31] A. L. Appleton, S. Barlow, S. R. Marder, K. I. Hardcastle, U. H. F. Bunz, *Synlett* **2011**, *22*, 1983–1986.
[32] B. D. Lindner, J. U. Engelhart, O. Tverskoy, A. L. Appleton, F. Rominger, A. Peters, H.-J. Himmel, U. H. F. Bunz, *Angew. Chem. Int. Ed.* **2011**, *50*, 8588–8591; *Angew. Chem.* **2011**, *123*, 8747–8750.
[33] J. U. Engelhart, B. D. Lindner, O. Tverskoy, F. Rominger, U. H. F. Bunz, *Org. Lett.* **2012**, *14*, 1008–1011.
[34] M. Müller, L. Ahrens, V. Brosius, J. Freudenberg, U. H. F. Bunz, *J. Mater. Chem. C* **2019**, *7*, 14011–14034.
[35] G. J. Richards, J. P. Hill, T. Mori, K. Ariga, *Org. Biomol. Chem.* **2011**, *9*, 5005–5017.
[36] Z. Liang, Q. Tang, R. Mao, D. Liu, J. Xu, Q. Miao, *Adv. Mater.* **2011**, *23*, 5514–5518.
[37] X.-K. Chen, J.-F. Guo, L.-Y. Zou, A.-M. Ren, J.-X. Fan, *J. Phys. Chem. C* **2011**, *115*, 21416–21428.
[38] T. Riehm, G. De Paoli, A. E. Konradsson, L. De Cola, H. Wadepohl, L. H. Gade, *Chem. Eur. J.* **2007**, *13*, 7317–7329.
[39] M. Matena, T. Riehm, M. Stöhr, T. A. Jung, L. H. Gade, *Angew. Chem. Int. Ed.* **2008**, *47*, 2414–2417; *Angew. Chem.* **2008**, *120*, 2448–2451.
[40] S. Blankenburg, E. Rauls, W. G. Schmidt, *J. Phys. Chem. Lett.* **2010**, *1*, 3266–3270.
[41] M. Matena, M. Stöhr, T. Riehm, J. Björk, S. Martens, M. S. Dyer, M. Persson, J. Lobo-Checa, K. Müller, M. Enache, H. Wadepohl, J. Zegenhagen, T. A. Jung, L. H. Gade, *Chem. Eur. J.* **2010**, *16*, 2079–2091.
[42] S. C. Martens, T. Riehm, S. Geib, H. Wadepohl, L. H. Gade, *J. Org. Chem.* **2011**, *76*, 609–617.
[43] S. C. Martens, U. Zschieschang, H. Wadepohl, H. Klauk, L. H. Gade, *Chem. Eur. J.* **2012**, *18*, 3498–3509.
[44] S. Geib, S. C. Martens, M. Märken, A. Rybina, H. Wadepohl, L. H. Gade, *Chem. Eur. J.* **2013**, *19*, 13811–13822.
[45] S. Geib, U. Zschieschang, M. Gsänger, M. Stolte, F. Würthner, H. Wadepohl, H. Klauk, L. H. Gade, *Adv. Funct. Mater.* **2013**, *23*, 3866–3874.
[46] L. Hahn, S. Öz, H. Wadepohl, L. H. Gade, *Chem. Commun.* **2014**, *50*, 4941–4943.
[47] S. Langbein, H. Wadepohl, L. H. Gade, *J. Org. Chem.* **2015**, *80*, 12620–12626.
[48] B. A. R. Günther, S. Höfener, U. Zschieschang, H. Wadepohl, H. Klauk, L. H. Gade, *Chem. Eur. J.* **2019**, *25*, 14669–14678.
[49] S. Höfener, B. A. R. Günther, M. E. Harding, L. H. Gade, *J. Phys. Chem. A* **2019**, *123*, 3160–3169.
[50] B. A. R. Günther, S. Höfener, R. Eichelmann, U. Zschieschang, H. Wadepohl, H. Klauk, L. H. Gade, *Org. Lett.* **2020**, *22*, 2298–2302.
[51] W. Yuan, J. Cheng, X. Li, M. Wu, Y. Han, C. Yan, G. Zou, K. Müllen, Y. Chen, *Angew. Chem. Int. Ed.* **2020**, *59*, 9940–9945; *Angew. Chem.* **2020**, *132*, 10026–10031.
[52] G. Seybold, G. Wagenblast, *Dyes Pigm.* **1989**, *11*, 303–317.
[53] J. H. Hurenkamp, W. R. Browne, R. Augulis, A. Pugžlys, P. H. M. van Loosdrecht, J. H. van Esch, B. L. Feringa, *Org. Biomol. Chem.* **2007**, *5*, 3354–3362.
[54] F. Würthner, V. Stepanenko, Z. Chen, C. R. Saha-Möller, N. Kocher, D. Stalke, *J. Org. Chem.* **2004**, *69*, 7933–7939.
[55] P. Rajasingh, R. Cohen, E. Shirman, L. J. W. Shimon, B. Rybtchinski, *J. Org. Chem.* **2007**, *72*, 5973–5979.
[56] L. Hahn, H. Wadepohl, L. H. Gade, *Org. Lett.* **2015**, *17*, 2266–2269.
[57] L. Hahn, F. Maaß, T. Bleith, U. Zschieschang, H. Wadepohl, H. Klauk, P. Tegeder, L. H. Gade, *Chem. Eur. J.* **2015**, *21*, 17691–17700.
[58] T. Okamoto, S. Kumagai, E. Fukuzaki, H. Ishii, G. Watanabe, N. Niitsu, T. Annaka, M. Yamagishi, Y. Tani, H. Sugiura, T. Watanabe, S. Watanabe, J. Takeya, *Sci. Adv.* **2020**, *6*, eaaz0632.
[59] F. Würthner, A. Sautter, C. Thalacker, *Angew. Chem. Int. Ed.* **2000**, *39*, 1243–1245; *Angew. Chem.* **2000**, *112*, 1298–1301.
[60] C. Lee, W. Yang, R. G. Parr, *Phys. Rev. B* **1988**, *37*, 785–789.
[61] A. D. Becke, *J. Chem. Phys.* **1993**, *98*, 5648–5652.
[62] P. J. Stephens, F. J. Devlin, C. F. Chabalowski, M. J. Frisch, *J. Phys. Chem.* **1994**, *98*, 11623–11627.
[63] F. Weigend, R. Ahlrichs, *Phys. Chem. Chem. Phys.* **2005**, *7*, 3297–3305.
[64] F. Weigend, *Phys. Chem. Chem. Phys.* **2006**, *8*, 1057–1065.
[65] S. Grimme, J. Antony, S. Ehrlich, H. Krieg, *J. Chem. Phys.* **2010**, *132*, 154104.
[66] S. Grimme, S. Ehrlich, L. Goerigk, *J. Comput. Chem.* **2011**, *32*, 1456–1465.
[67] J. T. Markiewicz, F. Wudl, *ACS Appl. Mater. Interfaces* **2015**, *7*, 28063–28085.
[68] Y. Ruiz-Morales, *J. Phys. Chem. A* **2002**, *106*, 11283–11308.
[69] E. Clar, R. Schoental, *Polycyclic hydrocarbons, Vol. 2*, Springer, Berlin, Heidelberg, **1964**, 1–487.
[70] E. Clar, *Aromatic Sextet*, John Wiley & Sons Ltd, London, **1972**, 1–146.
[71] R. Greiner, R. Blanc, C. Petermayer, K. Karaghiosoff, P. Knochel, *Synlett* **2016**, *27*, 231–236.
[72] B. Ferrier, N. Campbell, *J. Chem. Soc.* **1960**, 3513–3515.
[73] Y. Zhang, B. Illarionov, A. Bacher, M. Fischer, G. I. Georg, Q.-Z. Ye, D. Vander Velde, P. E. Fanwick, Y. Song, M. Cushman, *J. Org. Chem.* **2007**, *72*, 2769–2776.
[74] H. Höchstetter (Bayer AG), *Ger. Pat. Appl.*, DE 39 42 893A1 **1991**.
[75] J. Lee, S. J. Kim, H. Choi, Y. H. Kim, I. T. Lim, H.-M. Yang, C. S. Lee, H. R. Kang, S. K. Ahn, S. K. Moon, D.-H. Kim, S. Lee, N. S. Choi, K. J. Lee, *J. Med. Chem.* **2010**, *53*, 6337–6354.
[76] S. Cacchi, P. G. Ciattini, E. Morera, G. Ortar, *Tetrahedron Lett.* **1986**, *27*, 5541–5544.
[77] F. Würthner, *Pure Appl. Chem.* **2006**, *78*, 2341–2349.
[78] A. Dittmer, R. Izsák, F. Neese, D. Maganas, *Inorg. Chem.* **2019**, *58*, 9303–9315.
[79] I. Seguy, P. Jolinat, P. Destruel, R. Mamy, H. Allouchi, C. Courseille, M. Cotrait, H. Bock, *ChemPhysChem* **2001**, *2*, 448–452.
[80] V. Barone, M. Cossi, *J. Phys. Chem. A* **1998**, *102*, 1995–2001.
[81] M. Cossi, N. Rega, G. Scalmani, V. Barone, *J. Comput. Chem.* **2003**, *24*, 669–681.
[82] S. Stoll, *Electron Paramagnetic Resonance: Volume 22, Vol. 22*, The Royal Society of Chemistry, **2011**, pp. 107–154.
[83] G. Knizia, *J. Chem. Theory Comput.* **2013**, *9*, 4834–4843.
[84] G. R. Fulmer, A. J. M. Miller, N. H. Sherden, H. E. Gottlieb, A. Nudelman, B. M. Stoltz, J. E. Bercaw, K. I. Goldberg, *Organometallics* **2010**, *29*, 2176–2179.

Manuscript received: January 17, 2022
Accepted manuscript online: February 9, 2022
Version of record online: February 28, 2022